Net primary production annual maxima in the North Atlantic projected to shift in the 21st century.

Jenny Hieronymus[1], Magnus Hieronymus[1], Matthias Gröger[2], Jörg Schwinger[3], Raffaele Bernadello[4], Etienne Tourigny[4], Valentina Sicardi[4], Itzel Ruvalcaba Baroni[1], Klaus Wyser[1]

[1]Swedish Meteorological and Hydrological Institute, SMHI, Norrköping, 601 76, Sweden
[2]Department of Physical Oceanography and Instrumentation, Leibniz Institute for Baltic Sea Research Warnemünde, Rostock, D-18119, Germany
[3]NORCE Climate & Environment, Bjerknes Centre for Climate Research, Bergen, 5007, Norway
[4]Barcelona Supercomputing Center, BSC, Barcelona, 08034, Spain

Correspondence to: Jenny Hieronymus (jenny.hieronymus@smhi.se)

Abstract. Shifts in the day of peak Net Primary Production (NPP) were detected in different biogeochemical provinces of the North Atlantic (25-65° N). Most provinces displayed a shift towards earlier peak NPP with the largest change-points in the 21st century and in the northern parts of the domain. Furthermore, the occurrences of the first day with a Mixed Layer Depth (MLD) shallower than 40 m and the day of peak NPP are positively correlated over most of the domain. As was the case for the day of peak NPP, the largest changepoints for the day of MLD shallower than 40m occur around or after the year 2000. Daily output from two fully coupled CMIP6 Earth System Models, EC-Earth3-CC and NorESM2-LM, for the period 1750-2100 and under SSP5-8.5 scenario were used for the analysis. The ESM NPP data was compared to estimates derived from the CAFE satellite based data. The ESMs showed significant differences from the CAFE model though the timing of peak NPP was well captured for most provinces. The largest changepoints in the day of peak NPP occurs earlier in EC-Earth3-CC than in NorESM2-LM. Although SSP5-8.5 is a very high warming scenario, EC-Earth3-CC generates changepoints for most provinces in the early part of the 21st century, before the warming has deviated far from lower emission scenarios. NorESM2-LM displays the largest change-points centered around the mid 21st century with two out of 8 provinces displaying a largest change-point before the year 2050. The early timing of the detected shifts in some provinces in both ESMs suggests that similar shifts could already have been initiated or could start in the near future. This highlights the need for long term monitoring campaigns in the North Atlantic.

1 Introduction

Net Primary Production (NPP) is the rate of photosynthetic carbon fixation minus cellular respiration. In the ocean, the majority of NPP is performed by microscopic planktonic phototrophs. Though the individual plankton are small, the total marine NPP is

30 similar in size to its terrestrial counterpart with an estimated size of marine NPP on the order of 50PgC yr^{-1} (eg. Kulk et al., 2020, Westberry et al., 2008, Silsbe et al., 2016, Field et al., 1998). Phytoplankton constitutes the basis of the food chain and the carbon fixed through NPP provides the energy for higher trophic levels. Changes in NPP thus affect the entire ecosystem and ultimately fisheries and human food supply (Stock et al., 2017). In addition, NPP is the first step in the biological carbon pump, a set of processes by which carbon is exported from the surface to the deep ocean through the sinking of organic matter

35 (Lutz et al., 2007). Understanding how the NPP and the subsequent export of organic carbon from the euphotic zone will change in future climate is thus vital for evaluating future uptake of atmospheric carbon dioxide (Honjo et al., 2014).

The North Atlantic is a region of particular importance for carbon sequestration in the deep ocean (Goris et al. 2018; Baker et al., 2022). This region contributes about 0.55-1.94 PgC yr^{-1} (Sanders et al. 2014) to the global export production, estimated to

40 be 4-12 PgC yr^{-1} (de Vries and Weber, 2017). Moreover, cold water increases CO_2 solubility. Deep mixing and subduction in the subpolar North Atlantic thereby result in a net transport of carbon to depth, a combination of processes known as the solubility carbon pump.

NPP is affected by climate variability through precipitation, wind patterns, temperature and light and is thus projected to change

45 with anthropogenic climate change (Laufkötter et al., 2015; Paerl et al., 1999; Myriokefalitakis et al., 2020). Though an increase in temperature may enhance the growth rate of phytoplankton and thereby the net primary production, global NPP is projected to decrease (Behrenfeld et al., 2006; Steinacher et al., 2010; Bopp et al., 2013) though the uncertainty displayed in state-of-the-art Earth system Models (ESMs) is very large (Kwiatkowski et al., 2020). A projected NPP decline is often explained as being caused by increased water column stability that decreases the amount of nutrients available for primary

50 production (Behrenfeld et al., 2006; Steinacher et al., 2010) but processes such as retreat of sea ice and increased stratification in high latitudes reduces the light limitation leading to NPP increases (Kwiatkowski et al., 2020). Efforts have been made to estimate how NPP has already changed in the historical satellite record but the limited range of satellite time-series makes such endeavors difficult. Estimates range from -2.1% per decade over the period 1998-2015 (Gregg and Rousseaux, 2019) to no significant change (Kulk et al., 2020).

55

Several mechanisms have been hypothesized to explain the seasonal cycle of phytoplankton blooms. One often cited is the Critical Depth Hypothesis (Sverdrup, 1953) which postulates that a bloom can occur when the mixed layer has shoaled to a critical depth where the light limited gross production outweighs respiration. It does not, however, give an explanation as to when a bloom starts and ends. A more recent hypothesis, termed the Disturbance Recovery Theory, of the timing of blooms

60 was given by Behrenfeld (2010) (see also Behrenfeld and Boss, 2018). The hypothesis suggests a balance between the growth and the loss in terms of respiration, grazing and disturbances to the physical environment such as the depth of the mixed layer. Other hypotheses include Smyth et al. (2014) that relates the seasonality to the shift between negative and positive net heat flux.

The study of the timing of recurring biological events is termed "Phenology" and has become an important field of research during recent years due to its dependence on climate (Chivers et al., 2020). Phenological indicators include the seasonal length, the timing of start and end of bloom, and the timing of the annual maximum (eg. Nissen and Vogt, 2021; Henson et al., 2013). The phenology of algal blooms can change along with climate change with cascading effects into higher trophic levels up to fish and marine mammals. Changes in the phenology of phytoplankton blooms due to climate change have already been observed in the North Sea with the Continuous Plankton Recorder (CPR) since 1960, with data displaying a significantly earlier onset of the spring bloom (Chivers et al. 2020).

A phenological change in phytoplankton blooms will affect zooplankton and larvae as the timing of available food resources will change, an effect known as the match/mismatch hypothesis (Cushing, 1990, Durant et al., 2007). The suggested causes of phenological shifts range from bottom up controls, including thermal stratification occurring earlier in the year allowing for an earlier bloom initiation, to top down controls resulting from changes in zooplankton grazing pressure (Yamaguchi et al., 2022).

Henson et al. (2013) used historical simulations from six ESMs covering the years 1985-2009 and a high emission future scenario (RCP8.5) to study changes in the NPP phenology. They found a shift towards an earlier peak NPP for most areas around the globe. However, the monthly resolution of the CMIP5 data dampens the phenology signal considerably. In a more recent study, Henson et al. (2018) used higher frequency model output to investigate the effect of temporal resolution on results of phytoplankton phenology. They found that in order to detect long term trends in bloom timing, temporal resolution of 20 days or less is required.

However, even though a 20-day resolution may be adequate to detect long term trends, it is certainly not enough for detecting the timing of a rapid change in phenology in the course of global warming. In this paper, we use daily output from two ESMs that contributed to the 6th Coupled Model Intercomparison Project (Eyring et al., 2016), to investigate the evolution of oceanic net primary production and its phenology. The focus is a region 25-65° N in the North Atlantic during the period 1750-2100. We divide the domain into biogeochemical provinces (Longhurst et al., 1995) in order to see the evolution of NPP in different subregions across the domain. We then investigate the occurrence of change-points in the time-series of the day of peak NPP for the different provinces using change-point analysis.

To test how well the timing of mixed layer shoaling relates to the timing of peak NPP in different North Atlantic regions, we investigate the largest change-points also in the day of the mixed layer shoaling above a certain limit (here arbitrarily taken to be 40 m). We further analyse the cross-correlation between the day of mixed layer depth shallower than the limit and the day of peak NPP. The cross-correlation analysis is complementary to the change-point analysis. This analysis highlights at which leads and lags the timing of mixed layer shoaling and peak NPP are covariant in the different provinces.

2 Method

Daily output of vertically integrated NPP has been produced using NorESM2-LM and EC-Earth3-CC for 100 years of Pre-
100   industrial control (piControl), historical (1850-2014) and the very high emission scenario SSP5-8.5 (2015-2100, Kriegler et al.,
2017). The high emission scenario is chosen in order to generate a sort of upper end of the amount of change. Since daily data
require a lot of resources, no lower emission scenarios were run. Note that in EC-Earth3-CC, NPP is integrated over the entire
water column, while it is integrated over the top 100m in NorESM2-LM. All runs are forced with prescribed atmospheric CO_2
concentrations (concentration driven) in accordance with Meinshausen et al., 2020. The models are described in Sect. 2.1.
105   Section 2.2 describes the observational data set, Sect. 2.3, the Longhurst provinces and Sect. 2.4 provides an overview of the
change-point analysis method used. The phenological indicator that we have used is the day of peak NPP which is calculated as
the annual maximum of NPP. This is a well defined metric that is robust unless for bimodal distributions with two peaks of
similar size, which was not found in our data. The metric has previously been used in eg. Nissen and Vogt (2021) and Henson
et al. (2013).

110

The mixed layer depths used for the analysis are calculated differently in the two ESMs. In EC-Earth3-CC, we have used the
turbocline depth as a mixed layer depth proxy calculated with a turbulent mixing coefficient criterion of $5 cm^2 s^{-1}$ while in
NorESM2-LM, the mixed layer depth has been calculated in accordance with the criterion of de Boyer Montégut et al. (2004)
and with a density difference of $0.03 kg m^{-3}$.

115   ### 2.1 Models

2.1.1 EC-Earth3-CC

EC-Earth3 is an ESM developed by a European consortium of institutes and universities (Döscher et al. 2022). It is available in
several different configurations. For this work, we have used EC-Earth3-CC which consists of the Integrated Forecast System
(IFS) CY36R4 of the European Centre for Medium-Range Weather Forecasts (ECMWF) for simulating physics of the
120   atmosphere and land surface, NEMO3.6 (Madec et al., 2015) for ocean physics, LPJ-Guess (Smith et al., 2014) for terrestrial
vegetation and PISCES (Aumont et al., 2015) for ocean biogeochemistry. In concentration driven form, PISCES is fed a
spatially uniform atmospheric pCO_2 while a CO_2 mapping occurs within IFS to account for regional heterogeneities.

PISCES is a mixed Monod-quota model simulating two different phytoplankton functional types: diatoms and
125   nanophytoplankton, two size classes of zoo-plankton: micro and meso, and nutrients: nitrate, ammonium, phosphate, iron and
silicate. Iron and silicate are modeled using quotas in phytoplankton and the other nutrients with fixed Redfield ratios (Redfield,
1958). Phytoplankton growth depends on nutrient concentrations in ambient water, light and temperature. PISCES further

simulates the carbon system, as well as dissolved and particulate organic matter. The integrated net primary productivity used for the analysis is integrated over the water column and also summed over the two different phytoplankton functional types.

130

PISCES has been used and validated in a number of settings (Ramirez-romero et al., 2020; Gutknecht et al., 2019; Kwiatkowski et al., 2018). Skyllas et al. (2019) showed a good agreement between EC-Earth3 and temperature, salinity and nutrients and chlorophyll-a observations in an offline ocean-only version of NEMO-PISCES, for a north-south (29-63°N) transect in the Northwest Atlantic. Net primary production has not previously been validated for EC-Earth3-CC although the air-sea CO_2 flux,

135 which is strongly affected by net primary production, was compared to an observation based climatology in Döscher et al. (2022). Their results showed stronger uptake of CO_2 than observations in the North Atlantic, thought to be caused by too active convection in the Labrador Sea.

2.1.2 NorESM2-LM

140 The Norwegian Earth System Model NorESM2 (Seland et al., 2020, Tjiputra et al, 2020) is a fully coupled ESM, which is based on the Community Earth System Model version 2 (CESM2, Danabasoglu et al. 2020) but employs a different ocean component (the Bergen Layered Ocean Model, BLOM) and a modified atmosphere model (CAM6-Nor). The land surface and terrestrial biogeochemistry is represented by the Community Land Model version 5 (CLM5). BLOM uses isopycnic coordinates in the vertical (below a bulk mixed layer represented by two non-isopycnic model layers on top) and it includes the iHAMOCC

145 model to represent ocean biogeochemistry. BLOM is coupled to the sea-ice component CICE5, which is the same as in CESM2. The LM version of NorESM2 used in this study has an atmosphere-land resolution of 2° and a nominal ocean model resolution of 1°. iHAMOCC is derived from the HAMOCC model (Six and Maier-Reimer, 1996; Ilyina et al. 2013) and was adapted for the use with isopycnic coordinates by Assman et al. (2010). HAMOCC includes a relatively simple NPZD ecosystem model with one phytoplankton functional type, one zooplankton functional type, and an implicit representation of

150 calcifying and silicifying organisms. The model simulates the nutrients nitrate, phosphorus and dissolved iron with phytoplankton nutrient uptake according to Redfield molar ratios. The model also simulates the carbon system as well as dissolved and particulate organic matter. The growth of phytoplankton is further affected by light as well as temperature.

NorESM2-LM has been validated with regards to biogeochemical variables including net primary production in Tjiputra et al. (2020). The results show a seasonal cycle of marine NPP that is reasonably well captured in amplitude but with a too low annual mean.

2.2 Satellite based data - The CAFE model

Direct observational data records of net primary production are scarce and in order to validate the two ESMs with respect to NPP, we have chosen to use data from a satellite based approach. There are several different methods for deriving total water column NPP estimates from satellite data. Often they are either based on ocean color (Behrenfeld and Falkowski, 1997), carbon (Westberry et al., 2008) or absorption (Smyth et al., 2005).

In this work, we use data from the Carbon, Absorption and Fluorescence Euphotic-resolving (CAFE) model (Silsbe et al. 2016). The model utilizes satellite derived properties and has been shown to compare well to in situ observations (Johnson and Bif, 2021). We here utilize the MODIS-aqua (Moderate Resolution Imaging Spectroradiometer) dataset from 2002 to 2021.

2.3 Longhurst Provinces

The seasonality of NPP depends, among other things, on local physical ocean conditions. In modelling the terrestrial environment, the division into provinces of similar growth conditions, such as boreal forest or savannah, is well defined, while in the ocean, biological differences between regions exist but are more difficult to constrain (Sathyendranath et al., 1995). The division of the global ocean into biogeochemical provinces has been attempted several times (Longhurst et al., 1995; Sathyendranath et al., 1995) with the object of determining the global or regional net primary production. Longhurst et al. (1995) defined the static boundaries that we have used in this analysis. Although the boundaries in reality are shifting on seasonal and interannual time scales (Reygondeau et al., 2013), we have chosen to use the static boundaries as we then are able to compare the same localities in the two models and in the CAFE data. The North Atlantic is divided into the provinces shown in Fig. 1. Note that we have chosen not to include the entire Arctic basin causing the Arctic provinces to be cut off in the north. The boreal polar province (BPLR) is defined by the southward flowing Labrador current that continues northward along the Greenland coastline. The Atlantic Arctic province (ARCT) is defined by strong stratification caused by large inflow of meltwater while the Atlantic subarctic (SARC) is characterized by poleward flowing warm North Atlantic water. The Gulf

Stream (GFST), North Atlantic Drift (NADR), North West- (NASW) and North East Atlantic sub polar gyre (NASE) are governed by westerly winds and a Sverdrup type circulation. We have also included the coastal province North west Atlantic continental shelf (NWCS).

2.4 change-point analysis

change-point detection is a method to identify abrupt change in a time-series. Formally, the problem is to find the best possible segmentation of a signal according to some chosen criterion. Depending on this criterion one can look for changes in, for example, mean, variance, or a spectral characteristic of a given signal In climate science, the method has been used to detect shifts in a wide variety of quantities (Beaulieu et al., 2012) such as AMOC strength (Smeed et al., 2018), coastal organic carbon sequestration (Watanabe et al., 2019), and cod stock (Möllmann et al., 2021). We have used change-point detection to identify rapid change in the calendar-day of peak NPP. The calculations have been performed using the Python package Ruptures (Truong et al. 2020).

In general, change-point detection requires a search method, a cost function and a constraint on the number of change-points to detect. Search methods can be either exact or approximate. Here we use a version of the former called optimal detection, as computational speed is not an issue. Moreover, we use primarily the kernel based cost function and a constraint where we directly pick the desired number of change-points. Many methods of change-point analysis focus on finding a predetermined number of shifts in a predefined quantity, such as the time-series mean or variance (Truong et al., 2020). Another option is the PELT search method (Killick et al., 2012) that does not require the number of change-points to be determined beforehand. Instead, a penalty is defined that is related to the amplitude of the change of interest. A small penalty generates many change-points, which may arise due to intra-annual variability or noise, while a large penalty instead only gives the largest, if any, changes in the time-series. By choosing a large enough penalty, the number of change-points can in this way be tuned. In the process of doing this research we have tested both approaches.

Furthermore, instead of predefining the type of time-series change, we have chosen to primarily use a kernel based non-parametric cost function developed by Arlot et al. (2016), called "the kernel based cost function". This model can detect all types of changes in the probability distribution of the time-series; mean, variance and higher order changes such as skewness and kurtosis. The upside of this approach is that no large changes are missed. The downside is that the method does not provide

information on which change-point is related to what type of change. Therefore, we complement the method with analyses using the Least absolute deviation (L1) cost function that detects changes in the median and the Least squared deviation (L2) cost function that detects changes in the mean of the time-series. Both of these are also available through the Ruptures package and the search method used is the same as for the kernel based cost function.

3 Results

3.1 ESMs vs CAFE

We have compared the daily ESM data with 8 day NPP estimates from the CAFE data (Silsbe et al, 2016). Seasonal mean NPP over the MODIS-aqua period 2003-2021, for March, April, May (MAM) and June, July, August (JJA) are shown in Fig. 2. Note that the 2003-2021 period modelled by the ESMs is not the same period as that in the observationally constrained CAFE model. The two ESMs are forced with greenhouse gas concentrations that are similar to those for the period, but the internal variabilities of the two ESMs climate systems are not synchronised with nature or each other. The comparison that can be done is thus strictly climatological.

Figure 2 shows large spatial differences between CAFE, EC-Earth3-CC and NorESM2-LM data. Most notably, EC-Earth3-CC shows a very strong NPP in MAM over the Gulf stream region. The high resolution CAFE data show that the enhanced production occurs in the warm Gulf stream eddies while the low resolution of the ESMs gives a wider warm water transport. The NorESM2-LM results in the Gulf stream region are closer to the CAFE data, although the production in the northern part of the domain is underestimated in both ESMs.

The 8 day moving average of the area mean seasonal cycle over the period 2003-2021 for the different provinces is shown in Fig. 3. Due to the smaller area seen by satellites in winter, the CAFE data contains missing data over the winter months. In order to correctly compare the seasonal cycles, the ESM data was bounded to the north by the maximum latitude present in the CAFE data (Fig. S1).

The size of the NPP annual maxima as shown in Fig. 3 is well captured by both ESMs with the notable exception of the Gulf Stream province GFST in EC-Earth3-CC. This strong GFST production in EC-Earth3-CC is clearly seen in Fig. 2. However, the CAFE data shows a flatter and wider peak, indicating a longer growing season, which generates a higher mean NPP over the

time period compared to both ESMs for all provinces except for GFST and the North west Atlantic subtropical gyre, NASW, in EC-Earth3-CC (Tab. 1). It is also apparent from Fig. 3 that the timing of peak NPP differs between biogeochemical provinces and models (Tab. 1). In the CAFE data, the day of peak NPP occurs in day 164-178 (early to late June) in the northernmost provinces, BPLR, ARCT, SARC and NADR, while the subtropical gyres, NASW and NASE, the Gulf Stream, GFST, and the North west Atlantic shelf, NWCS, generates an earlier peak NPP between day 114 (April 24) and day 130 (May 10). Similarly, in EC-Earth3-CC, the three arctic provinces, BPLR, ARCT and SARC, display the latest peak NPP occurring from day 150 to day 166 (May 30 to June 15) while the peak NPP in the North Atlantic Drift, NADR, occurs earlier compared to CAFE (day 124, May 4). The earliest peak NPP occurs in the south eastern part of the domain, in NASE, on day 83 (March 24). As in the CAFE data, the earliest peak NPP in NorESM2-LM occurs in the North west subtropical gyre, NASW (April 26, day 116 compared to April 24 in CAFE), while the latest occurs in the continental shelf area, NWCS (day 186, July 5). In NorESM, the three arctic provinces display a day of peak NPP of 159 (June 8) for BPLR, 161 (June 10) for ARCT, and 176 (June 25) for SARC. The south eastern province, NASE, and the Gulf Stream province, GFST, have a day of peak NPP of 138 (May 18) and 148 (May 28) respectively. We note from Tab. 1, that the annual mean over this period is closer to CAFE in EC-Earth3-CC than in NorESM2-LM for all but one province (GFST) where the annual mean NPP is 38% higher than CAFE in EC-Earth3-CC and 37% lower than CAFE in NorESM2-LM. On the contrary, the day of peak NPP in this period is better captured by NorESM2-LM than EC-Earth3-CC in five out of eight provinces and is equally close to CAFE in one province (NASW). Here the day of peak NPP is 2 days later than CAFE in NorESM2-LM and 2 days earlier in EC-Earth3-CC. Only in two provinces, the continental shelf, NWCS, and GFST, is the day of peak NPP closer to CAFE in EC-Earth3-CC.

3.2 Historical and future NPP

The time-series of annual mean NPP for the different biogeochemical provinces from 100 years of piControl, historical and SSP5-8.5 are shown in Fig. 4 for EC-Earth3-CC, NorESM2-LM. Also shown in the annual mean CAFE data for the period 2003-2021. The figure reveals a large interannual and multidecadal variability in EC-Earth3-CC compared to NorESM2-LM.

For most provinces, EC-Earth3-CC generates higher annual mean NPP than NorESM2-LM, with the exception of the arctic province, BPLR, and the south eastern province, NASE. For BPLR, the mean for the entire period (not shown) is 110 mgC m^{-2}

day^{-1} for EC-Earth3-CC and 112 mgC m-2 day-1 for NorESM2-LM and for NASE 314mgC m^{-2} day^{-1} for EC-Earth3-CC

compared to 321mgC m^{-2} day^{-1} for NorESM2-LM. The largest difference between the two models is seen in the Gulf Stream,

GFST, where EC-Earth3-CC generates a time-series mean of 640 mgC m^{-2} day^{-1} compared to 282 mgC m^{-2} day^{-1} in NorESM2-

LM. The highest NPP in NorESM2-LM is instead found in the south eastern province, NASE.

265

The standard deviation for the entire period is in EC-Earth3-CC between 23.8 mgC m^{-2} day^{-1} and 71.6 mgC m^{-2} day^{-1} depending

on the province (not shown). The largest standard deviation is found in the eastern subtropical gyre, NASE, and the lowest in

the western continental shelf province, NWCS. In contrast, the standard deviation in NorESM2-LM is between 9.17 mgC m^{-2}

day^{-1} and 22.0 mgC m^{-2} day^{-1} with, similar to EC-Earth3-CC, the largest found in NASE and the lowest in NWCS.

270

In order to find how the NPP and the timing of peak NPP has changed over the time-series, we have compared the last 30 year

period of SSP5-8.5 (2070-2099, 2085s in the following) to the first 30 year period of the historical simulation (1850-1879,

1865s in the following). The results are summarized in Tab. 2. EC-Earth3-CC shows an increased NPP for most provinces with

the exception of the North Atlantic drift, NADR, and the south eastern NASE. Here, the NPP is lower in the 2085s compared

275   to the 1865s. In addition to those provinces, NorESM2-LM display decreased NPP also for western subtropical gyre, NASW,

and the subpolar province, SARC. The day of the year of peak NPP decreases for all provinces except one in both EC-Earth3-

CC (NASE) and NorESM2-LM (GFST).

To further find how the shift in phenology is distributed over the domain, the spatial distribution of the day of peak NPP

280   averaged over the 1865s for the two ESMs is shown in Fig. 5. Also shown in the figure is the difference of the ESM results

averaged over the period 1985-2014 (2000s in the following) and the 2085s from the 1865s. In the 1865s, both ESMs displayed

a pattern of later bloom in the northern parts compared to the rest of the domain. For EC-Earth3-CC, this is most notable in the

Labrador Sea while in NorESM2-LM, the later bloom is also visible in the Gulfstream and the northwest continental shelf area

(NWCS).

The 2000s show small and scattered differences from the 1865s. In the 2085s, most of the domain experienced an earlier peak NPP but with some notable exceptions. Parts around the Gulf stream display a markedly later peak NPP in the NorESM2-LM data compared to the 1865s. This corresponds to an expansion of the pattern of late peak NPP in the same area seen in the 1865s.

In EC-Earth3-CC, the pattern of earlier peak NPP in the final 30 years of SSP5-8.5 is widespread over the domain, although a notable feature is the much later bloom in the eastern subtropical gyre, NASE (27 days on average, Tab. 2). The NPP in this province was greatly reduced in the 2085s compared to the 1865s (-86.6 mgC m^{-2} day^{-1}, Tab. 2) caused by a strong reduction in winter surface nitrate concentration (not shown). The NPP seasonality in this area shifts from a clear spring peak to an extended

 period of weak NPP (not shown) with peak NPP therefore occurring later in the year. Also shown in Fig. 5 is the deviation of the 2085s from the 1865s mean divided by the standard deviation of the piControl in each grid cell which gives a measure of the significance of the 2085s change. A two-sample Kolmogorov-Smirnov test (KS-test, python routine `ks_2samp`) was done to compare the distributions for the 1865s and the 2085s. Areas where these distributions were not significantly at the 95% level are marked in the figure. The results show large significance in the northern parts of the domain while the KS-test generated no

 significant change on the 95 percentile for parts of the domain.

Taking the area average of each province allows us to look at the mean change in the day of peak NPP as well as identify change-points. Fig. 6 shows the time-series of the day of peak NPP averaged over the area of each province together with the largest (cf. Fig. S2 for the largest change-points using the PELT search method). In EC-Earth3-CC, the largest change-point

 occurs between 2002 (arctic provinces BPLR and ARCT) and 2066 (eastern subtropical gyre, NASE) for all provinces except the western subtropical gyre, NASW, where the largest change-point occurs the year 1900. Note also that NASW is the province with the least change over the time period (Tab. 2). In NorESM2-LM, the largest change-point is in general located

later, between 2010 (NASW) and 2082 (NASE). When increasing to two change-points, the pattern of most change occurring after the year 2000 is maintained with few change-points occurring earlier (Fig. 6). Also shown in the figure is the largest change-point found by the L1 and L2 cost function that indicates changes in the median and mean respectively. The results show that the L1, L2 and the kernel based cost function gives almost the same results for almost all provinces. The most discrepancy is found in the western subtropical gyre, NASW, in EC-Earth3-CC which is also the region displaying the least change.

Fig. 7 shows the first day of the year at which the spatial mean Mixed Layer Depth (MLD) shoals to 40 m or shallower in each province. Similar to the results of the day of peak NPP (Fig. 6), the day of MLD shallower than 40 m occurs progressively earlier over SSP5-8.5 for most provinces and for both EC-Earth3-CC and NorESM2-LM. The largest change-point in the time-series (Tab. 3) occurs between 1997 (Gulf stream, GFST) and 2067 (western subtropical gyre, NASW) for EC-Earth3-CC and between 2025 (arctic province, ARCT and the North Atlantic drift, NADR) and 2092 (western continental shelf, NWCS) for NorESM2-LM. Increasing to two change-points, the pattern is consistent with most points located after the year 2000 (Fig. 7). Note that the choice of 40 m is arbitrary. We have tested for other cut-off depths with similar results (Figs. S3-S5).

But how well do change-points in the spatial mean day of peak NPP of the different provinces represent the separate grid points? The year during which the largest change-point for every grid point occurs is shown in Fig. 8. The results broadly correspond to the results seen in the spatial mean time series with the largest change-points occurring after the year 2000. Few grid points display a change-point earlier than that. Note that many of the grid cells displaying change-points early in the time-series correspond to cells where the PELT search method could not find only one single change-point (Fig. S6). This points to the fact that in these grid points, little significant change occurs (cf. Fig. 5. bottom panel). Furthermore, EC-Earth3-CC displays an earlier largest change-point for most grid points as compared to NorESM2-LM. The northern part of the domain, where the euphotic zone is more vigorously coupled to the deep sea by vertical mixing like the Labrador Sea, northern North Atlantic and

the sub-polar gyre, shows the earliest change-point in the EC-Earth3-CC results close to the year 2000. The south-eastern part of the domain displays the latest change-point in both NorESM2-LM and EC-Earth3-CC.

To elucidate on the correlation between the day of MLD shallower than 40 m and the day of max NPP, the cross-correlation 335 (matlab routine `crosscorr`) between the time-series shown in Figs. 6 and 7 has been plotted in Fig. 9. The figure shows a notable correlation, well above the 95% confidence bound, between the two indices in most provinces for both ESMs. The maximum correlation occurs for zero lag in most provinces, indicating, as expected, that peaks in these variables tend to occur within the same year. Note that the strongest correlation for zero lag, at least in EC-Earth3-CC is seen in the west wind provinces, GFST, NADR, NASW and NASE that have a Sverdrup-like circulation. These are also open ocean provinces where 340 mixed layers can be expected to be less constrained by freshwater fluxes from land. Furthermore, a striking feature is the strong negative correlations found in the northern provinces, BPLR and ARCT, in EC-Earth3-CC. Looking at Fig. 7, we find that the day of MLD shallower than 40 m, at least in the BPLR province, occurs so early in the year that it can hardly affect the day of peak NPP. Thus, suggesting that the anti-correlation between these variables is owing to a hidden variable affecting both NPP and MLD. The similar correlation structure between BPLR and ARCT strongly suggests that the same is true about the ARCT 345 province.

4. Discussion

The comparison between CAFE and the two ESMs showed large differences between the three datasets (Fig. 2-3). However, the annual mean NPP is of the same order of magnitude and the day of peak NPP is well captured for most regions (Tab. 1). The regional difference in NPP is larger in the ESMs compared to the CAFE data which is evident by the difference in annual 350 mean between the provinces (Tab. 1). Peak NPP occurs latest in the year for the arctic provinces; BPLR, ARCT and SARC in EC-Earth3-CC which corresponds well to the CAFE data (although peak NPP in NADR occurs later than BPLR in CAFE).

Most provinces display an increased NPP over SSP5-8.5 for EC-Earth3-CC while for NorESM2-LM four provinces showed an NPP increase and four displayed a decrease (Fig. 4, Tab. 2). Averaged over the entire domain, NPP in EC-Earth3-CC is slightly
355   higher in the 2085s than in the 1865s and slightly lower in NorESM2-LM. The results are in line with the results of Tagliabue et al. (2021) that showed a 16 CMIP6 ESM mean NPP increase in the polar region, broadly corresponding to the Longhurst provinces BPLR, ARCT and SARC, where both EC-Earth3-CC and NorESM2-LM displays increased NPP between the 2085s and the 1865s (though NorESM2-LM displays a slight decrease in the subpolar province SARC). Note, however, that most of the increase presented in Tagliuabue et al. (2021) seems to occur higher up in the arctic than what is presented here. For the
360   regions presented in Tagliabue et al. (2021) that can be broadly compared to the rest of our domain, the CMIP6 model mean display a decline in NPP. Though only two out of five provinces in EC-Earth3-CC and three out of five provinces in NorESM2-LM display a decline, the decline is larger than the increase shown in the provinces displaying increased NPP (Tab. 2). Note also that the results presented in Tagliabue et al., relate to the reference period 1995-2014 which will impact the comparison to some degree. However, our results show little change before this period (Fig. 5) so the difference might not be that significant.

365

The results showed that the most change in the day of peak NPP, as well as in the day of MLD shallower than 40 m, occurs after the beginning of the 21st century (Figs. 6-8) which is consistent with the results of Henson et al. (2009), who found no long term trend in the subpolar North Atlantic towards earlier or later blooms in model data spanning 1959-2004. The earlier bloom displayed for most provinces (Tab. 2) under SSP5-8.5 is in agreement with Asch et al. (2019). They showed that blooms north
370   of 40°N shifted earlier under RCP8.5 using 5 daily output from GFDL ESM2M including the biogeochemical model TOPAZ2.0. In contrast, Henson et al. (2018) reports, using an ocean-only model (MEDUSA-2.0, NEMO), a start of bloom shifting later in the year under RCP8.5 in most parts of the North Atlantic. However, both studies relate to surface chlorophyll and not to NPP, which makes the comparison problematic. Although surface chlorophyll has the benefit of being easily validated to observations, it is not, in a simple manner, connected to vertically integrated NPP. The chlorophyll maxima can be
375   found below the surface (Cornec et al., 2021) and the relationship between the surface concentration and the subsurface profile differs between different localities (Sathyendranath et al., 1995). The seasonality of peak NPP is therefore not necessarily directly relatable to the seasonality of surface chlorophyll. Moreover, our temporal resolution is higher and both Henson et al. (2018) and Asch et al. (2019) use the start of bloom as well as length of bloom as a phenological indicator instead of the timing of the annual peak which further complicates the comparison.

380

In EC-Earth3-CC, the largest change-points in the day of peak NPP in many provinces occur already in the historical simulation, or in the early scenario simulation (Tab. 3), before the very high emission scenario SSP5-8.5 has started to diverge from the more moderate emission scenarios in terms of global mean surface temperature (O'Neill et al., 2016, Riahi et al., 2017). The effect of lower greenhouse gas concentrations on the locations of the change-points might therefore not be that large. These results point to significant phenological change that may have already started in this region and underlines the need of long-term monitoring campaigns in this area.

In NorESM2-LM, however, the largest change-points in the day of peak NPP occur later, in the mid to late 21st century (Tab. 3). Only in three provinces (the western subtropical gyre, NASW and the northern provinces, BPLR and SARC) the largest change-points occur before 2050. For NorESM2-LM a lower emission scenario might therefore generate even later change-points for most provinces. Note that the same change-points are generally found regardless of which cost function (L1,L2 or kernel based) is chosen in both models. This indicates that the change-points found are affecting multiple statistical moments.

The day of MLD shallower than 40m displays a similar pattern of the largest change-points generally occurring after the year 2000 (Tab. 3). We compared the day of peak NPP with the day of MLD shallower than 40 m and the cross-correlation did show the strongest correlation at zero lag. The fact that we saw significant correlations also with much longer lags likely reflected the low-frequency cycles of the Atlantic multi-decadal variability which affects many physical parameters, like SST and MLD, on multi-decadal time scales (e.g. Börgel et al. 2020). Both this type of low frequency variability and anthropogenic climate change could act as a hidden variable that through e.g. temperature and sea-ice changes, drives coherent changes in both NPP and MLD on a range of both positive and negative lags. Furthermore, we noted from Fig. 9 a strong anticorrelation between the MLD and NPP phenology for the arctic provinces BPLR and ARCT in EC-Earth3-CC. Given that both the provinces are far to the north and that SSP5-8.5 is a very strong warming scenario, we speculate that changes in sea-ice could be behind the observed correlation structure. This is supported by the fact that EC-Earth3 has been shown to overestimate sea ice concentrations in the Labrador Sea (Döscher et al., 2022). However, given that the timing of the MLD shallowing is unlikely to be important for the timing of peak NPP in these provinces we did not investigate further.

45

In both models and in nature, NPP and its timing is dependent on many other factors beyond the MLD, including light availability, nutrient concentrations and temperature. The MLD can similarly both be affected by and affect some of these factors. In light of this, MLD changes can both act as a driver of phenology changes in itself and act as a proxy for other drivers, which complicates the interpretation. The cross-correlation analysis therefore does not point to the validity of a certain bloom timing theory such as Critical Depth Hypothesis or the Disturbance Recovery Theory (Behrenfeld, 2010) but it does highlight the covariance of the NPP and MLD phenology.

The biogeochemical modules included in the Earth system models are by necessity simplistic, with PISCES simulating two phytoplankton functional types representing nanophytoplankton and diatoms and HAMOCC only one. However, even with reduced complexity interpretation is not straightforward. Compared to observations, community structure has been shown to affect the NPP and models containing a more dynamic phytoplankton community have a more non-linear response to climate change due to decreases in large cells and an increasing amount of regenerated production (Fu et al., 2016). Thus, more complex biogeochemical models may generate different results. The simpler biogeochemical model included in NorESM2-LM may be a factor in the lower variability seen in the NPP results (Fig. 4). Different phytoplankton functional types have been shown to react differently to climate change in the North Atlantic. Kléparski et al. (2023) found a decline in large flattened diatoms and an increase in biomass of elongated, slower sinking diatoms and dinoflagellates in six CMIP6 ESMs, which could influence the carbon export in this region.

For this work we have used fully coupled Earth system models as opposed to ocean-only models, that are often used for similar work (eg. Henson et al., 2018, 2009). The exchange of heat, momentum and freshwater is more accurately treated in coupled models than in ocean-only models. This affects, for example, temperature and stratification. It has also been demonstrated that interactive coupling affects the variability of these variables (e.g. Bhatt et al. 1998, Barsugli and Battisti, 1998). The biogeochemical response is therefore expected to differ in the coupled vs. the uncoupled case. Because of more consistent

physics with respect to uncoupled models, we believe using coupled models might constitute an important step forward in the larger effort of trying to understand what phenology changes might occur in the future.

The North Atlantic is a region of great importance for carbon sequestration through both the solubility pump and the biological pump (Baker et al., 2022). Our results show significant changes in the seasonality of peak NPP over large parts of the domain during the 21st century. These changes could in turn lead to trophic level decoupling and influence higher trophic levels (Yamaguchi et al., 2022) which are not yet modelled by the ESMs. In turn, this could impact the strength of the biological pump.

5 Summary and conclusions

In this work, we have shown that the seasonality of peak NPP in the North Atlantic (25-65°N) shifts earlier during the 21st century under SSP5-8.5 in two CMIP6 earth system models. The largest change towards an earlier day of peak NPP occurs in the northern parts of the domain for both ESMs. We separated the domain in biogeochemical provinces in accordance with Longhurst et al. (1995) in order to account for different local conditions. EC-Earth3-CC display change-points for many provinces already in the historical simulation, while the largest change-points in the NorESM2-LM data occur in the future scenario for all but one province (NASW), which is also the one displaying the least significant change. In EC-Earth3-CC, the largest change occurs in the biogeochemical province BPLR and in NorESM2-LM in the arctic province, ARCT. Moreover, the changes in the day of peak NPP are far outside the range of the natural variability diagnosed from the piControl run in large parts of the domain. The changing seasonality may have an impact on fishery yields through the mismatch of fish spawning and available resources. Furthermore, carbon sequestration in this highly productive domain may be affected by changes in ecosystem structure in turn affecting the export production and the general efficiency of the biological pump.

A comparison with the satellite based CAFE model showed that both ESMs display deviations from the CAFE data. At least for EC-Earth3-CC, this is especially true in the Gulf Stream region. NorESM2-LM is typically better at capturing the timing of peak NPP and EC-Earth3-CC is closer in annual average NPP in most provinces. The multi-decadal variability is smaller in

455   NorESM2-LM than in EC-Earth3-CC.

Cross-correlation analysis showed significant correlation between the day of MLD shallower than 40 m and the day of peak NPP in most provinces. The peak correlation occurs at zero lag, but correlations are significant at many both positive and negative lags. The large range of correlated lags we ascribe to forced and unforced low frequency variability affecting both

460   parameters. That is, the large range of correlated lags indicate that the NPP is likely controlled by other factors, in addition to MLD, that affect both variables. We also found evidence that these variables covary on multidecadal timescales indicating that low frequency internal- as well as forced climate variability affect these two parameters in similar ways.

We have presented results for two ESMs and for one future scenario. Including daily output of the 2-dimensional variable NPP

465   in standard CMIP runs would enable more thorough analysis of different models and scenarios. Since this variable is integrated over the water column it diminishes the risk of missing out on a deeper maxima which could be the case when investigating surface variables, such as surface chlorophyll, although we acknowledge the differences between, and importance of, both variables. Furthermore, though analysis of the high emission scenario gives us a sort of upper end on the changes we can expect, more moderate emission scenarios and more models would generate a span of possible shifts. The largest shifts in EC-

470   Earth3-CC occurring already in the historical simulation in many provinces indicates that seasonal shifts may already have started and highlights the importance of future work on including more models and scenarios in the analysis.

To conclude, the results presented in this work point to a shift towards earlier peak NPP for large parts of the North Atlantic (25°-65°N) in the 21st century, with most change occurring in the northern parts of the domain. Changes in primary production

475 phenology may impact entire ecosystems through a mismatch between zooplankton spawning and available resources (Cushing, 1990). Expanding this analysis with additional scenarios and models, preferably including more complex ecosystem dynamics, would constitute important future work.

480 **Code availability:** The EC-Earth3 code is available from the EC-Earth development portal for members of the consortium. All code related to CMIP6 forcing is implemented in the component models. Model codes developed at ECMWF, including the atmosphere model IFS, are intellectual property of ECMWF and its member states. Permission to access the EC-Earth3 source code can be requested from the EC-Earth community via the EC-Earth website (http://www.ec-earth.org/, EC-Earth consortium, 2019a) and may be granted if a corresponding software license agreement is signed with ECMWF. The repository
485 tag for the version of EC-Earth that is used in this work is 3.3.1. Currently, only European users can be granted access due to license limitations of the atmosphere model. The component models NEMO, LPJ-GUESS, TM5, and PISM are not limited by their licenses.

The NorESM code can be accessed via zenodo: Seland, Ø., Bentsen, M., Olivié, D., Toniazzo, T., Gjermundsen, A., Graff, L. S., Debernard, J. B., Gupta, A. K., He, Y., Kirkevåg, A., Schwinger, J., Tjiputra, J., Aas, K. S., Bethke, I., Fan, Y., Gao, S.,
490 Griesfeller, J., Grini, A., Guo, C., Ilicak, M., Karset, I. H. H., Landgren, O., Liakka, J., Moree, A., Moseid, K. O., Nummelin, A., Spensberger, C., Tang, H., Zhang, Z., Heinze, C., Iversen, T., and Schulz, M.: NorESM2 source code as used for CMIP6 simulations (includes additional experimental setups, extended model documentation, automated inputdata download, restructuring of BLOM/iHAMOCC input data), Zenodo [code], https://doi.org/10.5281/zenodo.3905091, 2020.

495 **Data availability:** The data used to produce the figures in this manuscript can be downloaded from Zenodo using the link: 10.5281/zenodo.10390601

The shape file defining the Longhurst provinces can be found there: https://www.marineregions.org/sources.php#longhurst (last access: Feb 5, 2024).

The CAFE data is freely available through the Ocean Productivity site:
500 http://sites.science.oregonstate.edu/ocean.productivity/index.php (last access: Nov 15, 2023).

The python package Ruptures can be downloaded from: https://centre-borelli.github.io/ruptures-docs/

Author contribution: JH performed the EC-Earth3-CC model run, made the analysis with contributions from MH, and drafted
505   the manuscript. MG contributed to the research design. JS performed the NorESM2-LM run. ET, RB and VS made the EC-Earth3-CC setup and contributed to the EC-Earth3-CC model run. IRB contributed with disscussions and paper writing. KW assisted in setting up and running EC-Earth3-CC. All co-authors contributed to the writing of the paper.

Competing interests: The authors declare that they have no conflict of interest.
510

Disclaimer: The work reflects only the author's/authors' view; the European Commission and their executive agency are not responsible for any use that may be made of the information the work contains.

Acknowledgements: The authors thank associate editor Stefano Ciavatta, reviewer Lee de Mora and one anonymous reviewer
515   for thorough reviews that have improved the quality of this work.

This project has received funding from the European Union's Horizon 2020 research and innovation programme under grant agreement No 820989 (project COMFORT, Our common future ocean in the Earth system – quantifying coupled cycles of carbon, oxygen, and nutrients for determining and achieving safe operating spaces with respect to tipping points). R. B. acknowledges support from the European Union's Horizon 2020 research and innovation programme under the Marie
520   Skłodowska-Curie grant agreement No GA 708063 (NetNPPAO).

References

Arlot, S., Celisse, A. and Harchaoui, Z. (2016). A kernel multiple change-point algorithm via model selection. hal-00671174v2f

Asch, R. G., Stock, C. A. and Sarmiento, J. L. (2019). Climate change impacts on mismatches between phytoplankton blooms and fish spawning phenology. Global Change Biology, 25(8), 2544–2559. https://doi.org/10.1111/gcb.14650

525   Assmann, K. M., Bentsen, M., Segschneider, J., and Heinze, C.: An isopycnic ocean carbon cycle model, Geoscientific Model Development, 3, 143–167, https://doi.org/10.5194/gmd-3-143-2010, 2010.

Aumont, O., Ethé, C., Tagliabue, A., Bopp, L., and Gehlen, M. (2015). PISCES-v2: An ocean biogeochemical model for carbon and ecosystem studies. Geoscientific Model Development, 8(8), 2465–2513. https://doi.org/10.5194/gmd-8-2465-2015

Baker, C. A., Martin, A. P., Yool, A., and Popova, E. (2022). Biological Carbon Pump Sequestration Efficiency in the North
530   Atlantic: A Leaky or a Long-Term Sink? Global Biogeochemical Cycles, 36(6). https://doi.org/10.1029/2021GB007286

60

Barsugli, J. J., and D. S. Battisti (1998). The Basic Effects of Atmosphere–Ocean Thermal Coupling on Midlatitude Variability. Journal of the Atmospheric Sciences, 55, 477–493, https://doi.org/10.1175/1520-0469(1998)055<0477:TBEOAO>2.0.CO;2

Bhatt, U. S., M. A. Alexander, D. S. Battisti, D. D. Houghton, and L. M. Keller (1998). Atmosphere–Ocean Interaction in the North Atlantic: Near-Surface Climate Variability. Journal of Climate, 11, 1615–1632, https://doi.org/10.1175/1520-0442(1998)011<1615:AOIITN>2.0.CO;2

Beaulieu, C., Chen, J. and Sarmiento, J. L. (2012). Change-point analysis as a tool to detect abrupt climate variations. Philosophical Transactions of the Royal Society A. 370. 1228–1249. http://doi.org/10.1098/rsta.2011.0383

Behrenfeld, M. J., and Falkowski, P. G. (1997). Photosynthetic rates derived from satellite-based chlorophyll concentration. Limnology and Oceanography, *42*(1), 1–20. https://doi.org/10.4319/lo.1997.42.1.0001

Behrenfeld, M. J., O'Malley, R. T., Siegel, D. A., McClain, C. R., Sarmiento, J. L., Feldman, G. C., Milligan, A. J., Falkowski, P. G., Letelier, R. M. and Boss, E. S. (2006). Climate-driven trends in contemporary ocean productivity. Nature, 444(7120), 752–755. https://doi.org/10.1038/nature05317

Behrenfeld, M. J. (2010). Abandoning Sverdrup's Critical Depth Hypothesis on phytoplankton blooms. Ecology, 91(4), 977–989. https://doi.org/10.1890/09-1207.1

Behrenfeld, M. J. and Boss, E. S. (2018). Student's tutorial on bloom hypotheses in the context of phytoplankton annual cycles. Global Change Biology, 24(1), 55–77. https://doi.org/10.1111/gcb.13858

Bopp, L., Resplandy, L., Orr, J. C., Doney, S. C., Dunne, J. P., Gehlen, M., Halloran, P., Heinze, C., Ilyina, T., Séférian, R., Tjiputra, J. and Vichi, M. (2013). Multiple stressors of ocean ecosystems in the 21st century: Projections with CMIP5 models. Biogeosciences, 10(10), 6225–6245. https://doi.org/10.5194/bg-10-6225-2013

550   Börgel, F., C. Frauen, T. Neumann, and H. E. M. Meier (2020). The Atlantic Multidecadal Oscillation controls the impact of the North Atlantic Oscillation on North European climate, Environmental Research Letters, https://doi.org/10.1088/1748-9326/aba925.

Chivers, W. J., Edwards, M. and Hays, G. C. (2020). Phenological shuffling of major marine phytoplankton groups over the last six decades. Diversity and Distributions, 26(5), 536–548. https://doi.org/10.1111/ddi.13028

555   Cornec, M., Claustre, H., Mignot, A., Guidi, L., Lacour, L., Poteau, A., et al. (2021). Deep chlorophyll maxima in the global ocean: Occurrences, drivers and characteristics. Global Biogeochemical Cycles, 35, e2020GB006759. https://doi.org/10.1029/2020GB006759

Cushing, D. H. (1990). Plankton Production and Year-class Strength in Fish Populations: an Update of the Match/Mismatch Hypothesis. Advances in Marine Biology, 26, 249-293. https://doi.org/10.1016/S0065-2881(08)60202-3

560   Danabasoglu, G., Lamarque, J. F., Bacmeister, J., Bailey, D. A., DuVivier, A. K., Edwards, J., Emmons, L. K., Fasullo, J., Garcia, R., Gettelman, A., Hannay, C., Holland, M. M., Large, W. G., Lauritzen, P. H., Lawrence, D. M., Lenaerts, J. T. M., Lindsay, K., Lipscomb, W. H., Mills, M. J., … Strand, W. G. (2020). The Community Earth System Model Version 2 (CESM2). Journal of Advances in Modeling Earth Systems, 12(2), 1–35. https://doi.org/10.1029/2019MS001916

de Boyer Montégut, C., Madec, G., Fischer, A. S., Lazar, A., and Iudicone, D. (2004). Mixed layer depth over the global ocean:
565   An examination of profile data and a profile-based climatology. Journal of Geophysical Research: Oceans, 109(12), 1–20. https://doi.org/10.1029/2004JC002378

DeVries, T., and T. Weber (2017), The export and fate of organic matter in the ocean: New constraints from combining satellite and oceanographic tracer observations, Global Biogeochem. Cycles, 31, 535–555, https://doi.org/10.1002/2016GB005551

65

Durant, J. M., Hjermann, D., Ottersen, G., and Stenseth, N. C. (2007). Climate and the match or mismatch between predator requirements and resource availability. Climate Research, 33(3), 271–283. https://doi.org/10.3354/cr033271

Döscher, R., Acosta, M., Alessandri, A., Anthoni, P., Arsouze, T., Bergman, T., Bernardello, R., Boussetta, S., Caron, L. P., Carver, G., Castrillo, M., Catalano, F., Cvijanovic, I., Davini, P., Dekker, E., Doblas-Reyes, F. J., Docquier, D., Echevarria, P., Fladrich, U., … Zhang, Q. (2022). The EC-Earth3 Earth system model for the Coupled Model Intercomparison Project 6. Geoscientific Model Development, 15(7), 2973–3020. https://doi.org/10.5194/gmd-15-2973-2022

Eyring, V., Bony, S., Meehl, G. A., Senior, C. A., Stevens, B., Stouffer, R. J., and Taylor, K. E. (2016). Overview of the Coupled Model Intercomparison Project Phase 6 (CMIP6) experimental design and organization, Geoscientific Model Development, 9, 1937–1958, https://doi.org/10.5194/gmd-9-1937-2016.

Field CB, Behrenfeld MJ, Randerson JT, Falkowski P (1998). Primary production of the biosphere: integrating terrestrial and oceanic components. Science. 281(5374):237-40. https://doi.org/10.1126/science.281.5374.237. PMID: 9657713.

Fu, W., Randerson, J. T., and Keith Moore, J. (2016). Climate change impacts on net primary production (NPP) and export production (EP) regulated by increasing stratification and phytoplankton community structure in the CMIP5 models. Biogeosciences, 13(18), 5151–5170. https://doi.org/10.5194/bg-13-5151-2016

Gregg, W. W., and Rousseaux, C. S. (2019). Global ocean primary production trends in the modern ocean color satellite record (1998-2015). Environmental Research Letters, 14(12). https://doi.org/10.1088/1748-9326/ab4667

Goris, N., Tjiputra, J. F., Olsen, A., Schwinger, J., Lauvset, S. K., and Jeansson, E. (2018). Constraining projection-based estimates of the future North Atlantic carbon uptake. Journal of Climate, 31(10), 3959–3978. https://doi.org/10.1175/JCLI-D-17-0564.1

70

Gutknecht, E., Reffray, G., Mignot, A., Dabrowski, T., and Sotillo, M. G. (2019). Modelling the marine ecosystem of Iberia-Biscay-Ireland (IBI) European waters for CMEMS operational applications. Ocean Science, 15(6), 1489–1516.

590   https://doi.org/10.5194/os-15-1489-2019

Henson, S. A., Dunne, J. P., and Sarmiento, J. L. (2009). Decadal variability in North Atlantic phytoplankton blooms. Journal of Geophysical Research: Oceans, 114(4), 1–11. https://doi.org/10.1029/2008JC005139

Henson, S., Cole, H., Beaulieu, C., and Yool, A. (2013). The impact of global warming on seasonality of ocean primary production. Biogeosciences, 10(6), 4357–4369. https://doi.org/10.5194/bg-10-4357-2013

595   Henson, S. A., Cole, H. S., Hopkins, J., Martin, A. P., and Yool, A. (2018). Detection of climate change-driven trends in phytoplankton phenology. Global Change Biology, 24(1), e101–e111. https://doi.org/10.1111/gcb.13886

Honjo, S., Eglinton, T. I., Taylor, C. D., Ulmer, K. M., Sievert, S. M., Bracher, A., German, C. R., Edgcomb, V., Francois, R., Deboraiglesias-Rodriguez, M., Van Mooy, B., and Repeta, D. J. (2014). The role of the biological pump in the global carbon cycle understanding an imperative for ocean science. Oceanography, 27(3), 10–16. https://doi.org/10.5670/oceanog.2014.78

600   Ilyina, T., Six, K. D., Segschneider, J., Maier-Reimer, E., Li, H., and Núñez-Riboni, I. (2013). Global ocean biogeochemistry model HAMOCC: Model architecture and performance as component of the MPI-Earth system model in different CMIP5 experimental realizations. JAMES, 5(2), 287–315. https://doi.org/10.1029/2012MS000178

Johnson, K. S., and Bif, M. B. (2021). Constraint on net primary productivity of the global ocean by Argo oxygen measurements. Nature Geoscience, 14(10), 769–774. https://doi.org/10.1038/s41561-021-00807-z

605   Killick, R., Fearnhead, P., and Eckley, I. A. (2012). Optimal detection of changepoints with a linear computational cost. Journal of the American Statistical Association, 107(500):1590–1598,107(500):1590–1598.
https://doi.org/10.1080/01621459.2012.737745

Kléparski, L., Beaugrand, G., Edwards, M., and Ostle, C. (2023). Phytoplankton life strategies, phenological shifts and climate change in the North Atlantic Ocean from 1850 to 2100. Global Change Biology, 29(13), 3833–3849.

610 https://doi.org/10.1111/gcb.16709

Kriegler, E., Bauer, N., Popp, A., Humpenöder, F., Leimbach, M., Strefler, J., Baumstark, L., Bodirsky, B. L., Hilaire, J., Klein, D., Mouratiadou, I., Weindl, I., Bertram, C., Dietrich, J. P., Luderer, G., Pehl, M., Pietzcker, R., Piontek, F., Lotze-Campen, H., … Edenhofer, O. (2017). Fossil-fueled development (SSP5): An energy and resource intensive scenario for the 21st century. Global Environmental Change, 42, 297–315. https://doi.org/10.1016/j.gloenvcha.2016.05.015

615 Kulk, G., Platt, T., Dingle, J., Jackson, T., Jönsson, B. F., Bouman, H. A., Babin, M., Brewin, R. J. W., Doblin, M., Estrada, M., Figueiras, F. G., Furuya, K., González-Benítez, N., Gudfinnsson, H. G., Gudmundsson, K., Huang, B., Isada, T., Kovač, Ž., Lutz, V. A., … Sathyendranath, S. (2020). Primary production, an index of climate change in the ocean: Satellite-based estimates over two decades. Remote Sensing, 12(5), 1–26. https://doi.org/10.3390/rs12050826

Lutz, M. J., Caldeira, K., Dunbar, R. B., and Behrenfeld, M. J. (2007). Seasonal rhythms of net primary production and
620 particulate organic carbon flux to depth describe the efficiency of biological pump in the global ocean. Journal of Geophysical Research: Oceans, 112(10). https://doi.org/10.1029/2006JC003706

Kwiatkowski, L., Aumont, O., Bopp, L., and Ciais, P. (2018). The Impact of Variable Phytoplankton Stoichiometry on Projections of Primary Production, Food Quality, and Carbon Uptake in the Global Ocean. Global Biogeochemical Cycles, 32(4), 516–528. https://doi.org/10.1002/2017GB005799

625 Kwiatkowski, L., Torres, O., Bopp, L., Aumont, O., Chamberlain, M., Christian, J., Dunne, J., Gehlen, M., Ilyina, T., John, J., Lenton, A., Li, H., Lovenduski, N., Orr, J., Palmieri, J., Schwinger, J., Séférian, R., Stock, C., Tagliabue, A., … Ziehn, T. (2020). Twenty-first century ocean warming, acidification, deoxygenation, and upper ocean nutrient decline from CMIP6 model projections. Biogeosciences. 17, 3439–3470. https://bg.copernicus.org/articles/17/3439/2020/

75

Laufkötter, C., Vogt, M., Gruber, N., Aita-Noguchi, M., Aumont, O,. Bopp, L., Buitenhuis, E., Doney, S. C., Dunne, J.,

630   Hashioka, T., Hauck, J. (2015). Drivers and uncertainties of future global marine primary production in marine ecosystem

models. Biogeosciences. 7;12(23):6955-84. https://doi.org/10.5194/bg-12-6955-2015

Longhurst, A., Sathyendranath, S., Platt, T. and Caverhill, C. (1995). An estimate of global primary production in the ocean

from satellite radiometer data. Journal of Plankton Research, 17(6), 1245–1271. https://doi.org/10.1093/plankt/17.6.1245

Lutz, M. J., Caldeira, K., Dunbar, R. B., and Behrenfeld, M. J. (2007). Seasonal rhythms of net primary production and

635   particulate organic carbon flux to depth describe the efficiency of biological pump in the global ocean. Journal of Geophysical

Research: Oceans, 112(10). https://doi.org/10.1029/2006JC003706

Madec, G. (2015). NEMO ocean engine, Note du Pole de modelisation de l'Institut Pierre-Simon Laplace No 27, ISSN No

1288-1619.

Meinshausen, M., Vogel, E., Nauels, A., Lorbacher, K., Meinshausen, N., Etheridge, D. M., Fraser, P. J., Montzka, S. A.,

640   Rayner, P. J., Trudinger, C. M., Krummel, P. B., Beyerle, U., Canadell, J. G., Daniel, J. S., Enting, I. G., Law, R. M., Lunder,

C. R., O'Doherty, S., Prinn, R. G., Reimann, S., Rubino, M., Velders, G. J. M., Vollmer, M. K., Wang, R. H. J., and Weiss, R.

(2017). Historical greenhouse gas concentrations for climate modelling (CMIP6), Geoscientific Model Development, 10, 2057–

2116, https://doi.org/10.5194/gmd-10-2057-2017.

Myriokefalitakis, S., Gröger, M., Hieronymus, J., and Döscher, R.: An explicit estimate of the atmospheric nutrient impact on

645   global oceanic productivity, Ocean Science, 16, 1183–1205, https://doi.org/10.5194/os-16-1183-2020, 2020.

Möllmann, C., Cormon, X., Funk, S., Otto, S. A., Schmidt, J. O., Schwermer, H., Sguotti, C., Voss, R., and Quaas, M. (2021).

Tipping point realized in cod fishery. Scientific Reports, 11(1), 1–12. https://doi.org/10.1038/s41598-021-93843-z

Nissen, C., and Vogt, M. (2021). Factors controlling the competition between Phaeocystis and diatoms in the Southern Ocean and implications for carbon export fluxes. Biogeosciences, 18(1), 251–283. https://doi.org/10.5194/bg-18-251-2021

650 O'Neill, B. C., Tebaldi, C., Van Vuuren, D. P., Eyring, V., Friedlingstein, P., Hurtt, G., Knutti, R., Kriegler, E., Lamarque, J. F., Lowe, J., Meehl, G. A., Moss, R., Riahi, K., and Sanderson, B. M. (2016). The Scenario Model Intercomparison Project (ScenarioMIP) for CMIP6. Geoscientific Model Development, 9(9), 3461–3482. https://doi.org/10.5194/gmd-9-3461-2016

Paerl, H.W., Willey, J. D., Go, M., Peierls, B. L., Pinckney, J. L., Fogel, M. L. (1999). Rainfall stimulation of primary production in western Atlantic Ocean waters: roles of different nitrogen sources and co-limiting nutrients. Marine Ecology Progress Series. 18;176:205-14. https://doi.org/10.3354/meps176205

655

Ramirez-romero, E., Jordà, G., Amores, A., Kay, S., Segura-noguera, M., Macias, D. M., Maynou, F., Sabatés, A., and Alexander, M. A. (2020). Assessment of the Skill of Coupled Physical – Biogeochemical Models in the NW Mediterranean. 7(July), 1–18. https://doi.org/10.3389/fmars.2020.00497

Redfield, A. C. (1958). The biological control of chemical factors in the environment. American Scientist, 46(3), 205–221. 660 https://doi.org/10.5194/bg-11-1599-2014

Reygondeau, G., Longhurst, A., Martinez, E., Beaugrand, G., Antoine, D., and Maury, O. (2013). Dynamic biogeochemical provinces in the global ocean. Global Biogeochemical Cycles, 27(4), 1046–1058. https://doi.org/10.1002/gbc.20089

Riahi, K., van Vuuren, D. P., Kriegler, E., Edmonds, J., O'Neill, B. C., Fujimori, S., Bauer, N., Calvin, K., Dellink, R., Fricko, O., Lutz, W., Popp, A., Cuaresma, J. C., KC, S., Leimbach, M., Jiang, L., Kram, T., Rao, S., Emmerling, J., … Tavoni, M. 665 (2017). The Shared Socioeconomic Pathways and their energy, land use, and greenhouse gas emissions implications: An overview. Global Environmental Change, 42, 153–168. https://doi.org/10.1016/j.gloenvcha.2016.05.009

Sanders, R., Henson, S. A., Koski, M., De La Rocha, C. L., Painter, S. C., Poulton, A. J., Riley, J., Salihoglu, B., Visser, A., Yool, A., Bellerby, R., and Martin, A. P. (2014). The Biological Carbon Pump in the North Atlantic. Progress in Oceanography, 129(PB), 200–218. https://doi.org/10.1016/j.pocean.2014.05.005

670   Sathyendranath, S., Longhurst, A., Caverhill, C. M., and Platt, T. (1995). Regionally and seasonally differentiated primary production in the North Atlantic. Deep-Sea Research Part I, 42(10), 1773–1802.   https://doi.org/10.1016/0967-0637(95)00059-F

Seland, Ø., Bentsen, M., Olivié, D., Toniazzo, T., Gjermundsen, A., Graff, L. S., Debernard, J. B., Gupta, A. K., He, Y. C., Kirkevåg, A., Schwinger, J., Tjiputra, J., Schanke Aas, K., Bethke, I., Fan, Y., Griesfeller, J., Grini, A., Guo, C., Ilicak, M., …

675   Schulz, M. (2020). Overview of the Norwegian Earth System Model (NorESM2) and key climate response of CMIP6 DECK, historical, and scenario simulations. In Geoscientific Model Development (Vol. 13, Issue 12). https://doi.org/10.5194/gmd-13-6165-2020

Silsbe, G. M., Behrenfeld, M. J., Halsey, K. H., Milligan, A. J., and Westberry, T. K. (2016). The CAFE model: A net production model for global ocean phytoplankton. Global Biogeochemical Cycles, 30(12), 1756–1777.

680   https://doi.org/10.1002/2016GB005521

Six, K. D. and Maier-Reimer, E. (1996). Effects of plankton dynamics on seasonal carbon fluxes in an ocean general circulation model, Global Biogeochemical Cycles, 10, 559–583. https://doi.org/10.1029/96GB02561

Skyllas, N., Bintanja, R., Buma, A. G. J., Brussaard, C. P. D., Gröger, M., Hieronymus, J., and van de Poll, W. H. (2019). Validation of stratification-driven phytoplankton biomass and nutrient concentrations in the northeast atlantic ocean as

685   simulated by EC-earth. Geosciences (Switzerland), 9(10). https://doi.org/10.3390/geosciences9100450

Smeed, D. A., Josey, S. A., Beaulieu, C., Johns, W. E., Moat, B. I., Frajka-Williams, E., Rayner, D., Meinen, C. S., Baringer, M. O., Bryden, H. L., and McCarthy, G. D. (2018). The North Atlantic Ocean Is in a State of Reduced Overturning. Geophysical Research Letters, 45(3), 1527–1533. https://doi.org/10.1002/2017GL076350

Smith, B., Wårlind, D., Arneth, A., Hickler, T., Leadley, P., Siltberg, J., and Zaehle, S. (2014). Implications of incorporating N
690   cycling and N limitations on primary production in an individual- based dynamic vegetation model, Biogeosciences, 11, 2027–2054, https://doi.org/10.5194/bg-11-2027-2014, 2014.

Smyth, T. J., Tilstone, G. H., and Groom, S. B. (2005). Integration of radiative transfer into satellite models of ocean primary production. Journal of Geophysical Research: Oceans, 110(10), 1–11. https://doi.org/10.1029/2004JC002784

Smyth T. J., Allen I., Atkinson A., Bruun J., T., Harmer R. A., et al. (2014). Ocean Net Heat Flux Influences Seasonal to
695   Interannual Patterns of Plankton Abundance. PLOS ONE 9(6): e98709. https://doi.org/10.1371/journal.pone.0098709

Steinacher, M., Joos, F., Frölicher, T. L., Bopp, L., Cadule, P., Cocco, V., Doney, S. C., Gehlen, M., Lindsay, K., Moore, J. K., Schneider, B., and Segschneider, J. (2010). Projected 21st century decrease in marine productivity: A multi-model analysis. Biogeosciences, 7(3), 979–1005. https://doi.org/10.5194/bg-7-979-2010

Stock, C. A., John, J. G., Rykaczewski, R. R., Asch, R. G., Cheung, W. W. L., Dunne, J. P., Friedland, K. D., Lam, V. W. Y.,
700   Sarmiento, J. L., and Watson, R. A. (2017). Reconciling fisheries catch and ocean productivity. Proceedings of the National Academy of Sciences of the United States of America, 114(8), E1441–E1449. https://doi.org/10.1073/pnas.1610238114

Sverdrup, H. U. (1953). On conditions for the vernal blooming of phytoplankton. ICES Journal of Marine Science, 18(3), 287–295. https://doi.org/10.1093/icesjms/18.3.287

Tagliabue A, Kwiatkowski L, Bopp L, Butenschön M, Cheung W, Lengaigne M and Vialard J (2021). Persistent Uncertainties in Ocean Net Primary Production Climate Change Projections at Regional Scales Raise Challenges for Assessing Impacts on Ecosystem Services. Frontiers in Climate. 3:738224. https://doi.org/10.3389/fclim.2021.738224

Tjiputra, J. F., Schwinger, J., Bentsen, M., L. Morée, A., Gao, S., Bethke, I., Heinze, C., Goris, N., Gupta, A., He, Y. C., Olivié, D., Seland, O., and Schulz, M. (2020). Ocean biogeochemistry in the Norwegian Earth System Model version 2 (NorESM2). Geoscientific Model Development, 13(5), 2393–2431. https://doi.org/10.5194/gmd-13-2393-2020

Truong, C., Oudre, L., and Vayatis, N. (2020). Selective review of offline change-point detection methods. Signal Processing, 167. https://doi.org/10.1016/j.sigpro.2019.107299

Watanabe, K., Seike, K., Kajihara, R., Montani, S., and Kuwae, T. (2019). Relative sea-level change regulates organic carbon accumulation in coastal habitats. Global Change Biology, 25(3), 1063–1077. https://doi.org/10.1111/gcb.14558

Westberry, T., Behrenfeld, M. J., Siegel, D. A., and Boss, E. (2008). Carbon-based primary productivity modeling with vertically resolved photoacclimation. Global Biogeochemical Cycles, 22(2), 1–18. https://doi.org/10.1029/2007GB003078

Yamaguchi, R., Rodgers, K. B., Timmermann, A., Stein, K., Schlunegger, S., Bianchi, D., Dunne, J. P., and Slater, R. D. (2022). Trophic level decoupling drives future changes in phytoplankton bloom phenology. Nature Climate Change, 12(5), 469–476. https://doi.org/10.1038/s41558-022-01353-1
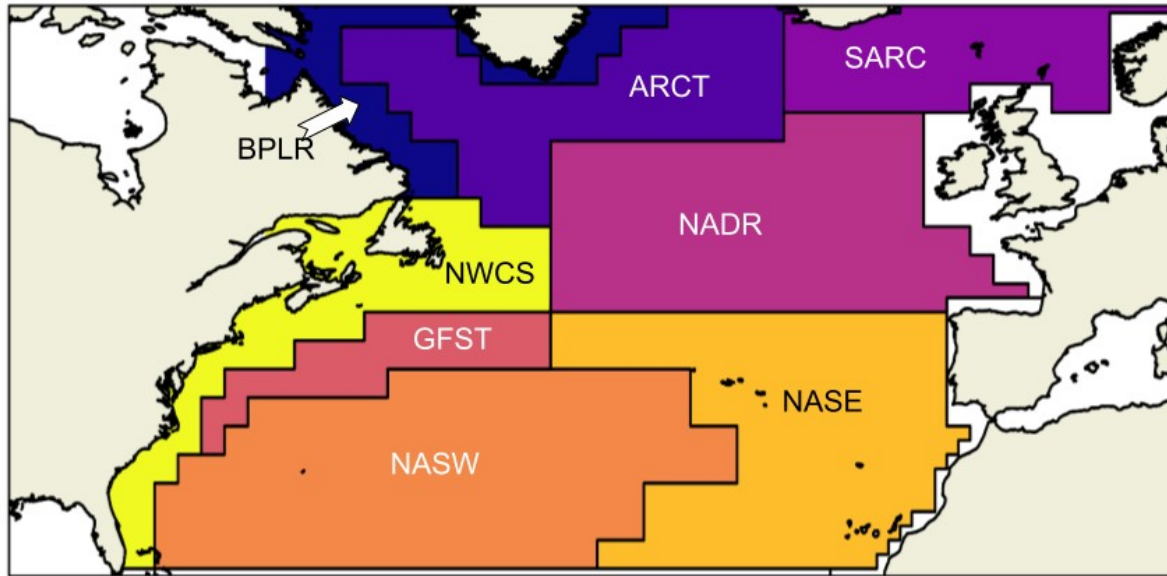
90

Figure 1: Study area and Longhurst provinces. BPLR: Boreal polar, ARCT: Atlantic arctic, SARC: Atlantic subarctic, NADR: North Atlantic drift, GFST: Gulf stream, NASW: North west Atlantic subtropical gyre, NASE: North east Atlantic subtropical gyre, NWCS North west Atlantic shelf.

720

725

Figure 2: Vertically integrated seasonal mean NPP from the CAFE model (upper), EC-Earth3-CC (middle) and NorESM2-LM
(bottom) for March, April, May (MAM, left) and for June, July, August (JJA, right). The difference between the contours is 100 mgC
m^{-2} day^{-1}
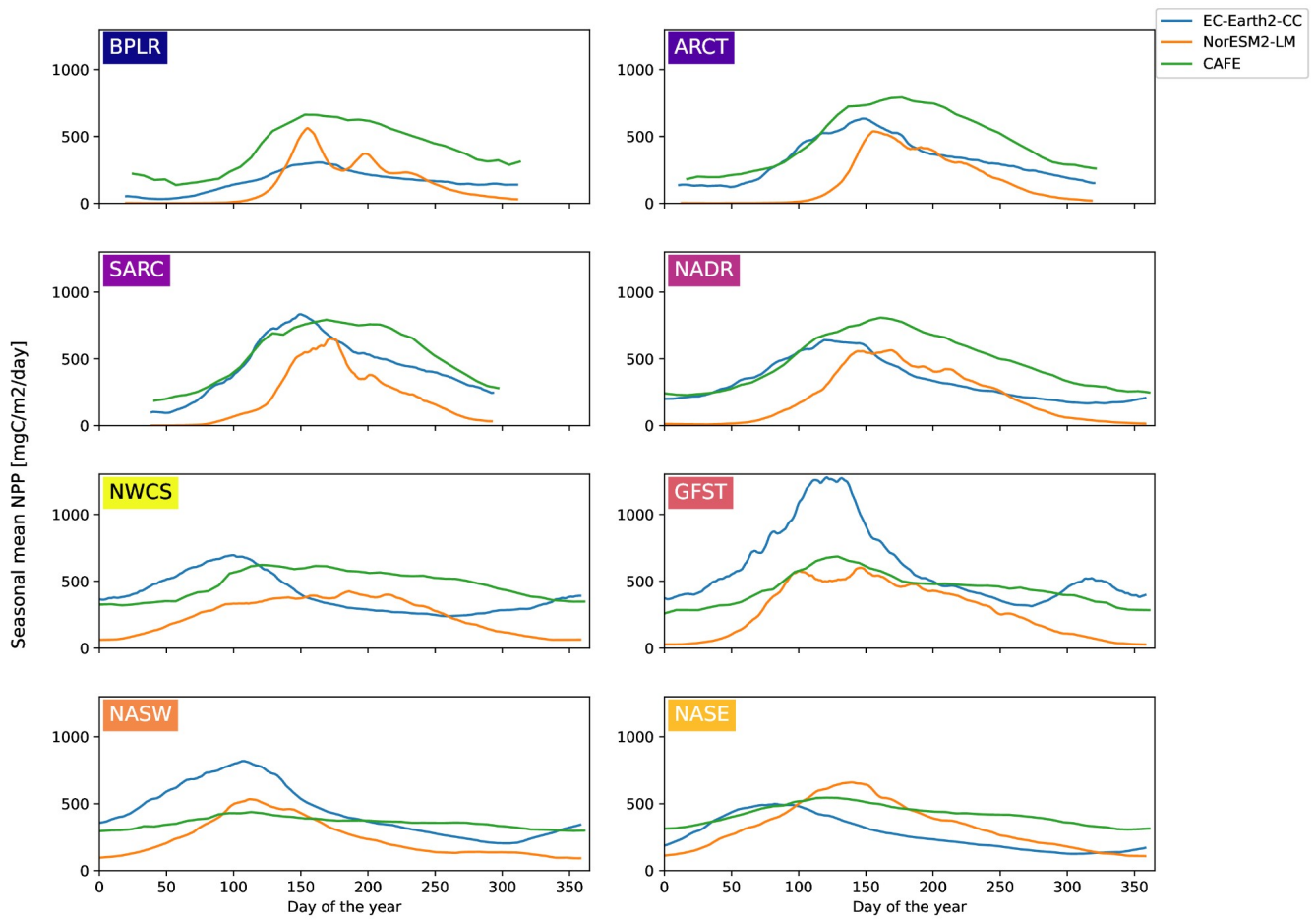
Figure 3: Seasonal cycles of vertically integrated NPP for CAFE (green), EC-Earth3-CC(blue) and NorESM2-LM(orange) for the different provinces shown in Fig. 1. The model data was masked by the maximum latitude present in the CAFE data to account for the smaller winter domain visible by satellites. A multi-year (2003-2021) average is shown. The ESM data is an 8 day moving average.

100

Province	CAFE		EC-Earth3-CC		NorESM2-LM	
	Mean NPP [mgC m^{-2} day^{-1}]	Day of peak NPP	Mean NPP [mgC m^{-2} day^{-1}]	Day of peak NPP	Mean NPP [mgC m^{-2} day^{-1}]	Day of peak NPP
BPLR	405	155	161	166	141	159
ARCT	470	179	321	152	160	161
SARC	525	171	442	150	210	176
NADR	472	163	332	124	203	172
NWCS	477	122	396	100	239	186
GFST	441	130	608	126	276	148
NASW	358	114	442	112	238	116
NASE	419	122	273	83	326	138
Total	424	161	371	121	242	153

Table 1. Mean NPP and mean Day of peak NPP over the time period 2003-2021 for the different provinces shown in Fig.

1. Also shown is the mean values averaged over the entire domain (Total). The ESM data was masked to the real valued

745   CAFE data.
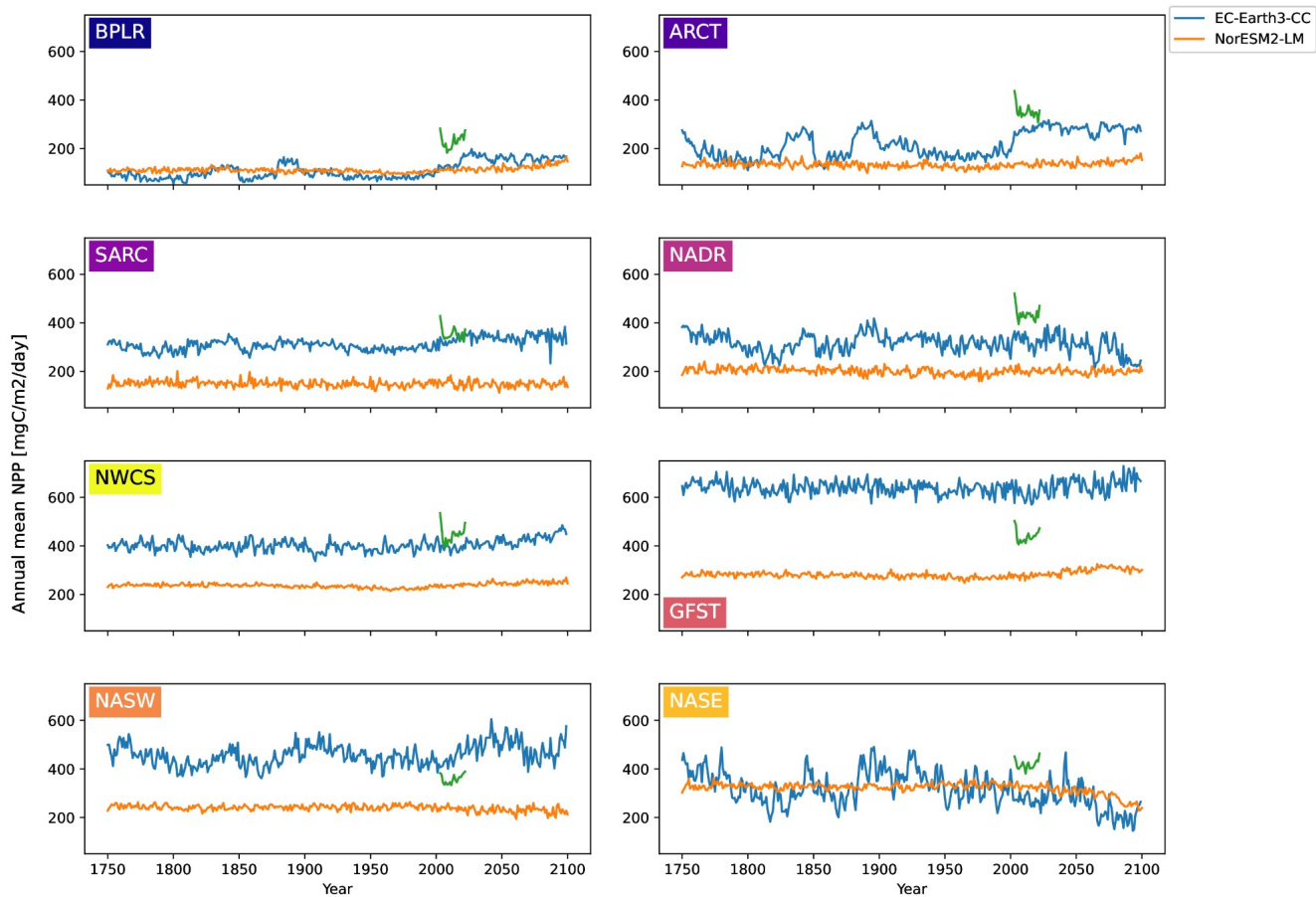
Figure 4: Time-series of annual mean vertically integrated NPP for the different biogeochemical provinces for EC-Earth3-CC (blue), NorESM2-LM (orange) and CAFE (green).

Province	EC-Earth3-CC 2070 to 2099 (2085s) mean minus 1850 to 1889 (1865s) mean		NorESM2-LM 2070 to 2099 (2085s) mean minus 1850 to 1889 (1865s) mean	
	NPP [mgC m^{-2} day^{-1}]	Day of peak NPP	NPP [mgC m-2 day-1]	Day of peak NPP
BPLR	79.4	-68.2	24.7	-12.09
ARCT	125	-25.8	15.4	-20.8
SARC	48.6	-8.84	-2.25	-18.0
NADR	-24.1	-7.71	-3.19	-10.1
NWCS	42.8	-12.7	12.2	-1.40
GFST	20.4	-5.73	28.0	13.3
NASW	47.4	-5.13	-14.1	-1.28
NASE	-86.6	27.0	-59.8	-12.8
Total	12.9	-3.91	-12.4	-7.48

Table 2. Mean NPP over the period 2070-2099 minus mean NPP over the period 1850-1889 together with the difference in the day of peak NPP for the same periods. Also shown in the corresponding value averaged over the entire domain (Total).
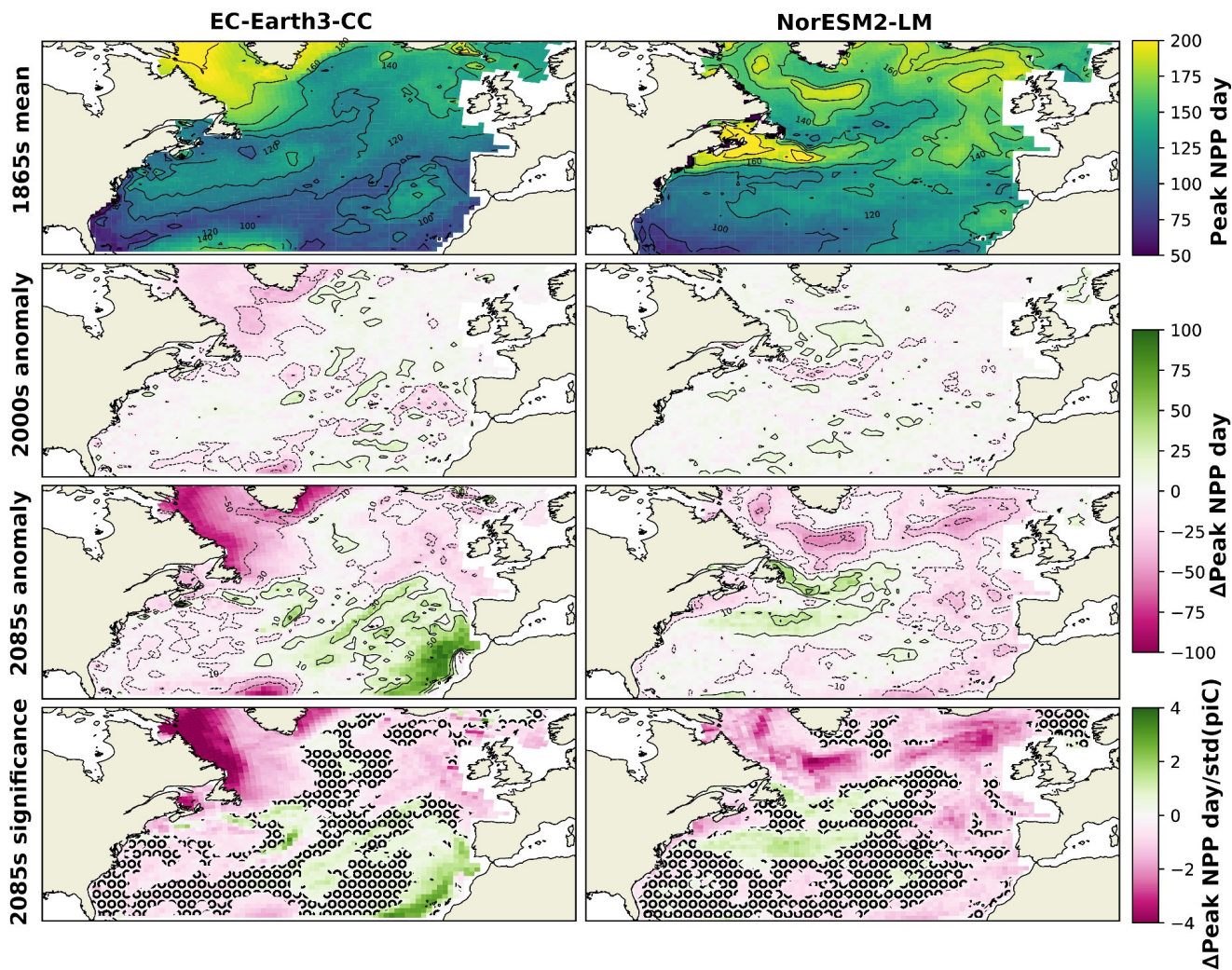
Figure 5: Mean day of peak NPP for NorESM2-LM (left) and EC-Earth3-CC (right) over the years 1850-1879 (top). The second panels show the mean over 1985-2014 minus the 1850-1879 mean. The third panels shows the mean over 2070-2099 minus the 1850-1879 mean (bottom). The bottom panels show the results from the third panels normalised by the yearly standard deviation of the day of peak NPP in the respective piControl simulations, giving a view of how large the changes are compared to unforced variability. Grid cells that do not show significance on the 95 percentile are marked with a black ring pattern. The difference between the contour lines is 20 days.
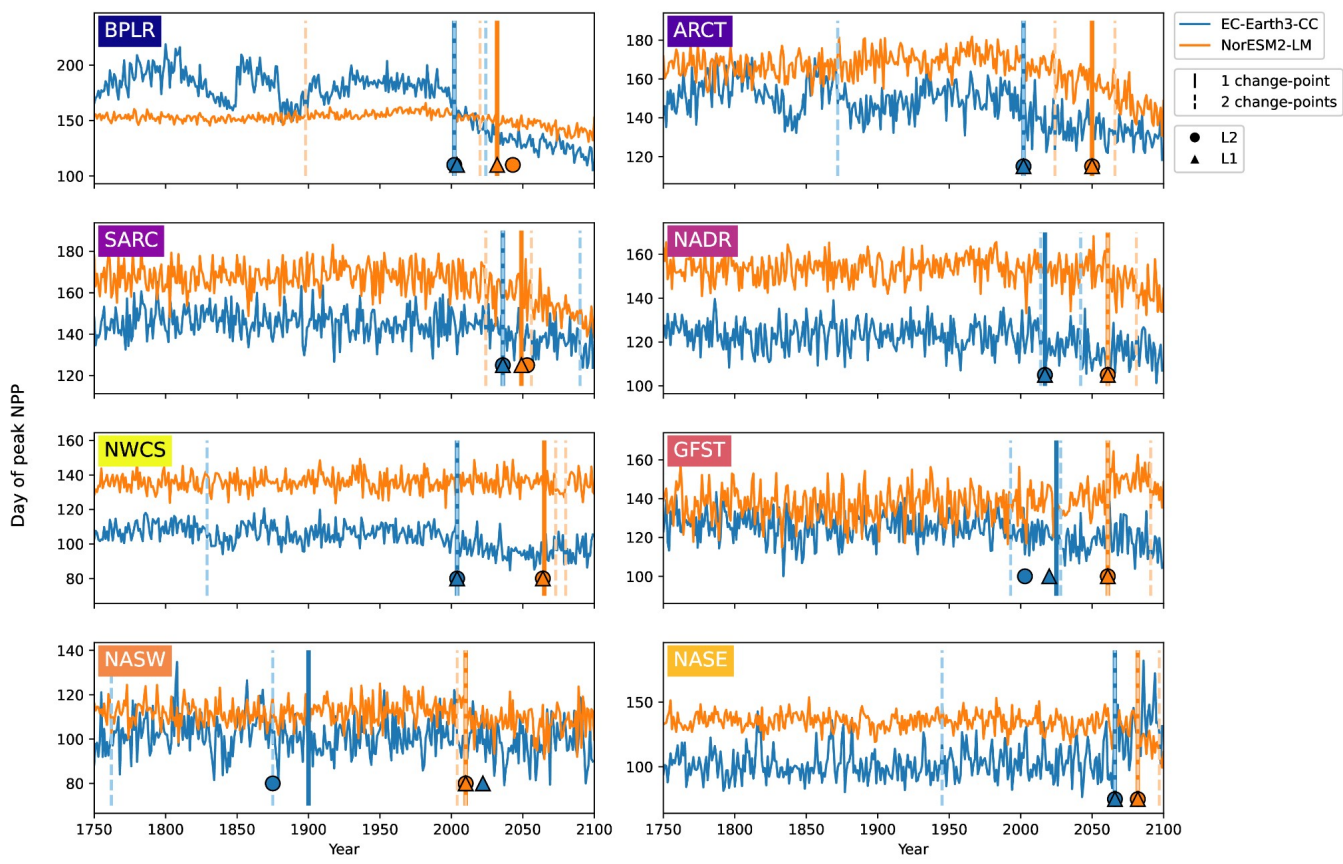
Figure 6: Day of peak NPP per province for EC-Earth3-CC (blue) and NorESM2-LM (orange). Note the differing y-axes. The largest change-points (calculated with a kernel based cost function) in the time-series are marked by the vertical lines. The single largest change-point is marked by solid lines and the two largest are marked with dashed lines. The centre of the circles represents the largest change-point in the time series that corresponds to a change in the mean (L2) while the centre of the triangles represents the largest change-point corresponding to a change in the median (L1).
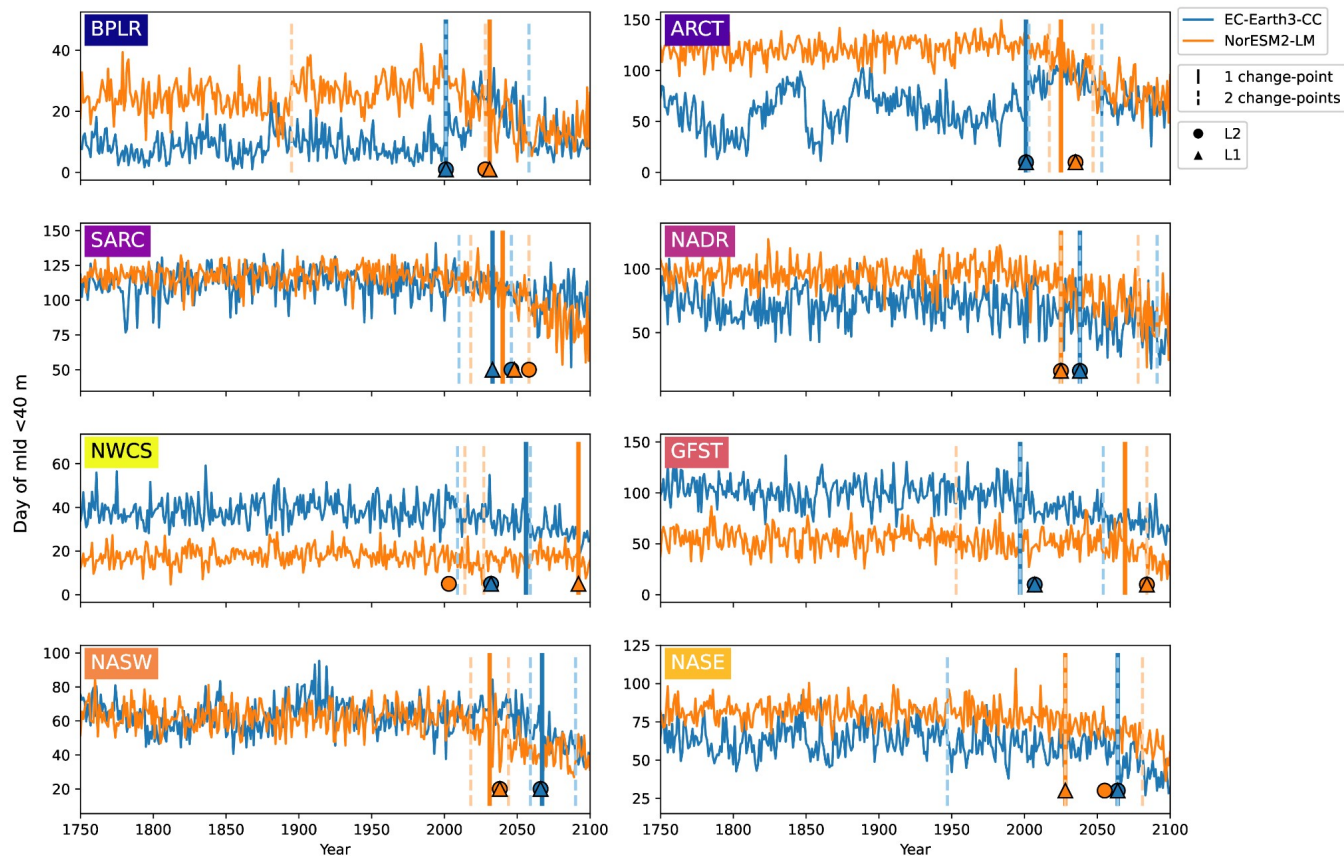
Figure 7: First day of the year when the mixed layer is 40m or less for EC-Earth3-CC (blue) and NorESM2-LM (orange). Note the differing y-axes. The largest change-points (calculated with a kernel based cost function) in the time-series are marked by the vertical lines. The single largest change-point is marked by solid lines and the two largest are marked with dashed lines. The centre of the circles represents the largest change-point in the time series that corresponds to a change in the mean (L2) while the centre of the triangles represents the largest change-point corresponding to a change in the median (L1).

Province	EC-Earth3-CC Largest change-point [year]		NorESM2-LM Largest change-point [year]	
	Day of peak NPP	Day of MLD <40m	Day of peak NPP	Day of MLD <40m
BPLR	2002	2001	2032	2031
ARCT	2002	2001	2050	2025
SARC	2036	2033	2049	2040
NADR	2017	2038	2061	2025
NWCS	2004	2056	2065	2092
GFST	2025	1997	2061	2069
NASW	1900	2067	2010	2031
NASE	2066	2064	2082	2028

Table 3. The table shows the largest change-points of the day of peak NPP and the day of MLD<40m time series for the different provinces shown in Fig. 1.

790

120
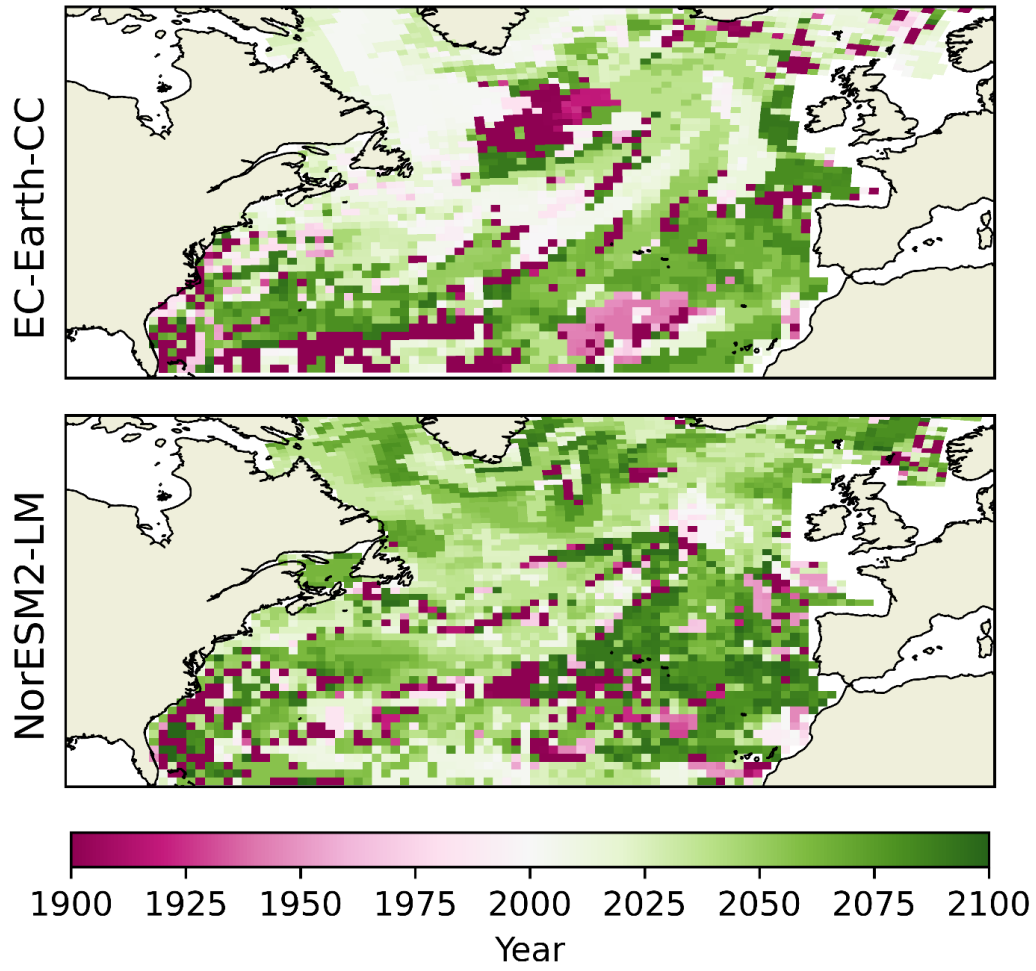
Figure 8: Year of change-point of the day of maximum primary production for all grid spaces. The change-point algorithm is here set to look for only one change-point.

795
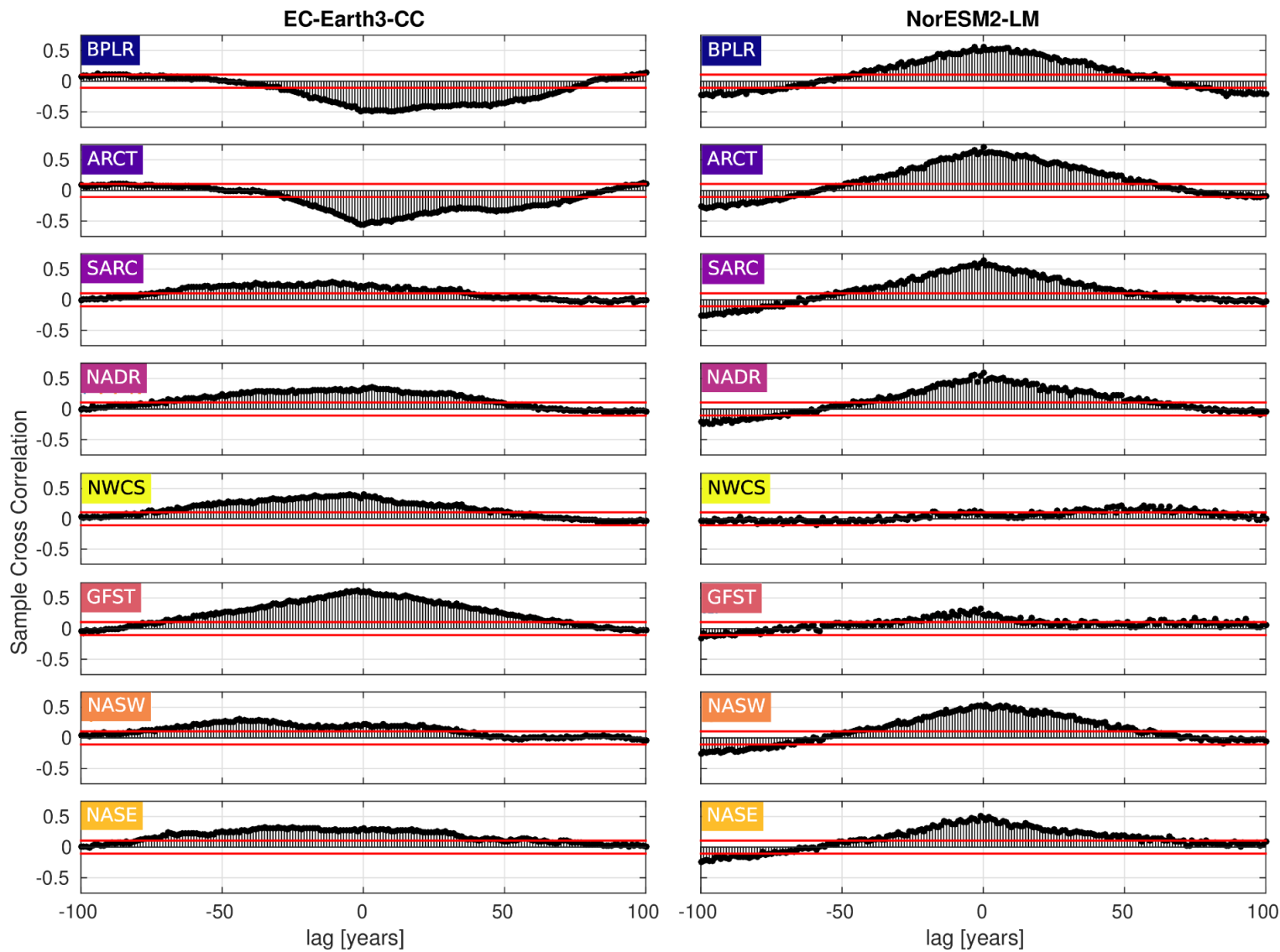
Figure 9: Cross-correlation between the day of peak NPP and the first day of mixed layer depth (MLD) shallower than or equal to 40m. Negative lag means that the day of peak NPP proceeds the first day of MLD shallower than 40m, while the opposite holds for positive lag. The horizontal blue lines mark the 95% confidence bounds.